The Astrophysical Journal, 639:1227–1237, 2006 March 10

ALUMINUM-MAGNESIUM AND OXYGEN ISOTOPE STUDY OF RELICT Ca-Al-RICH INCLUSIONS IN CHONDRULES

Alexander N. Krot,[1] Kevin D. McKeegan,[2] Gary R. Huss,[1,3] Kurt Liffman,[1,4,5] Sandeep Sahijpal,[6] Ian D. Hutcheon,[7] Gopalan Srinivasan,[8] Adolph Bischoff,[9] and Klaus Keil[1]

Received 2004 December 3; accepted 2005 September 27

ABSTRACT

Relict Ca-Al-rich inclusions (CAIs) in chondrules crystallized before their host chondrules and were subsequently partly melted together with chondrule precursors during chondrule formation. Like most CAIs, relict CAIs are ^{16}O enriched ($\Delta^{17}O < -20‰$) compared to their host chondrules ($\Delta^{17}O > -9‰$). Hibonite in a relict CAI from the ungrouped carbonaceous chondrite Adelaide has a large excess of radiogenic ^{26}Mg (^{26}Mg*) from the decay of ^{26}Al, corresponding to an initial $^{26}Al/^{27}Al$ ratio [$(^{26}Al/^{27}Al)_I$] of $(3.7 \pm 0.5) \times 10^{-5}$; in contrast, melilite in this CAI and plagioclase in the host chondrule show no evidence for ^{26}Mg* [$(^{26}Al/^{27}Al)_I$ of $<5 \times 10^{-6}$]. Grossite in a relict CAI from the CH carbonaceous chondrite PAT 91546 has little ^{26}Mg*, corresponding to a $(^{26}Al/^{27}Al)_I$ of $(1.7 \pm 1.3) \times 10^{-6}$. Three other relict CAIs and their host chondrules from the ungrouped carbonaceous chondrite Acfer 094, CH chondrite Acfer 182, and H3.4 ordinary chondrite Sharps do not have detectable ^{26}Mg* [$(^{26}Al/^{27}Al)_I < 1 \times 10^{-5}$, $<(4-6) \times 10^{-6}$, and $<1.3 \times 10^{-5}$, respectively]. Isotopic data combined with mineralogical observations suggest that relict CAIs formed in an ^{16}O-rich gaseous reservoir before their host chondrules, which originated in an ^{16}O-poor gas. The Adelaide CAI was incorporated into its host chondrule after ^{26}Al had mostly decayed, at least 2 Myr after the CAI formed, and this event reset ^{26}Al-^{26}Mg systematics.

Subject heading: solar system: formation

1. INTRODUCTION

One of the major questions in cosmochemistry concerns the age relationship of Ca-Al-rich inclusions (CAIs) and chondrules,[10] which are some of the earliest objects to form in the solar nebula (Amelin et al. 2002, 2004) and which together are the dominant component in chondritic meteorites (chondrites). This age relationship provides the major constraints on the chronology of the solar nebula and can be potentially established using the short-lived radionuclide ^{26}Al ($t_{1/2} = 0.73$ Myr), which was present in the nebular regions where CAIs and chondrules formed (e.g., MacPherson et al. 1995; Russell et al. 1996). Based on the observations that most CAIs appear to have formed with a $(^{26}Al/^{27}Al)_I$ of $\sim(5-7) \times 10^{-5}$ (e.g., MacPherson et al. 1995; Bizzarro et al. 2004; Young et al. 2005), often called "canonical," whereas the most ^{26}Al-rich chondrules apparently formed with a $(^{26}Al/^{27}Al)_I \leq 1.2 \times 10^{-5}$, it is often inferred that CAIs formed at least 1.5 Myr before the majority of chondrules (Russell et al. 1996; Kita et al. 2000, 2005; McKeegan et al. 2000; Marhas et al. 2000; Huss et al. 2001; Mostefaoui et al. 2002). This chronological interpretation is based on the assumption that ^{26}Al had a stellar origin and was injected into and homogenized within the solar nebula over a timescale that was short compared to its half-life (MacPherson et al. 1995; Goswami et al. 2005).

The alternative, nonchronological interpretation of the differences in the $(^{26}Al/^{27}Al)_I$ ratios of CAIs and chondrules assumes a local origin of ^{26}Al by energetic particle (protons, ^{3}He, and ^{4}He) irradiation near the proto-Sun, resulting in radial heterogeneity of the ^{26}Al distribution in the solar nebula (Gounelle et al. 2001; Goswami et al. 2005 and references therein). According to this model, refractory inclusions formed in the reconnection ring, <0.02 AU from the proto-Sun, where they were subjected to extensive energetic particle irradiation. Chondrules formed contemporaneously with CAIs farther away from the proto-Sun, in the protoplanetary disk, where they were largely shielded from irradiation and acquired a lower abundance of ^{26}Al than CAIs (Shu et al. 1996, 2001; Gounelle et al. 2001).

Compound objects composed of a chondrule and a refractory inclusion can potentially provide the best constraints on the relative timing of CAI and chondrule formation, because both constituents of the compound objects were affected by the same heating episode in the same solar nebula region. These objects can be divided into two categories—relict chondrules inside igneous CAIs (Itoh & Yurimoto 2003; Krot et al. 2005a) and relict CAIs inside chondrules (e.g., Misawa & Nakamura 1988).

Calcium-aluminum-rich inclusions enclosing chondrule-like material are exceptionally rare; only three have been described so far—a melilite-rich igneous (compact type A) CAI enclosing low-Ca pyroxene and high-Ca pyroxene grains in Yamato-81020 (CO3.0; Itoh & Yurimoto 2003) and two anorthite-rich igneous CAIs (type C) enclosing fragments of forsteritic olivine intergrown

[1] Hawai'i Institute of Geophysics and Planetology, School of Ocean and Earth Science and Technology, University of Hawai'i at Manoa, Honolulu, HI 96822; sasha@higp.hawaii.edu.
[2] Department of Earth and Space Sciences, University of California, Los Angeles, CA 90095.
[3] Department of Geological Sciences and Center for Meteorite Studies, Arizona State University, Tempe, AZ 85287-1404.
[4] School of Mathematical Sciences, Monash University, VIC 3800, Australia.
[5] Commonwealth Scientific and Industrial Research Organisation, Manufacturing and Infrastructure Technology, Highett, VIC 3190, Australia.
[6] Department of Physics, Panjab University, Chandigarh 160014, India.
[7] Lawrence Livermore National Laboratory, Livermore, CA 94451.
[8] Department of Geology, University of Toronto, Toronto, ON M5S 3B1, Canada.
[9] Institut für Planetologie, Universität Münster, 48149 Münster, Germany.
[10] CAIs are 0.1–10 mm sized, irregularly shaped or rounded objects composed mostly of oxides and silicates of Ca, Al, Ti, and Mg, such as corundum (Al_2O_3), hibonite ($CaAl_{12}O_{19}$), grossite ($CaAl_4O_7$), perovskite ($CaTiO_3$), spinel ($MgAl_2O_4$), Al,Ti-pyroxene (solid solution of $CaTi^{+4}Al_2O_6$, $CaTi^{+3}AlSiO_6$, $CaAl_2SiO_6$, and $CaMgSi_2O_6$), melilite (solid solution of $Ca_2MgSi_2O_7$ and $Ca_2Al_2SiO_7$), and anorthite ($CaAl_2Si_2O_8$). Chondrules are igneous, rounded objects, 0.01–10 mm in size, composed largely of ferromagnesian olivine ($Mg_{2-x}Fe_xSiO_4$) and pyroxene ($Mg_{1-x}Fe_xSiO_3$, where $1 < x < 0$), Fe,Ni-metal, and glassy or microcrystalline mesostasis.

with low-Ca pyroxene in Allende (CV3; Krot et al. 2005a). These compound objects have been interpreted in different ways: Itoh & Yurimoto (2003) concluded that chondrule-like material inside the Yamato-81020 CAI formed prior to the host CAI formation, whereas Krot et al. (2005a) concluded that the two Allende type C CAIs experienced late-stage remelting ($\sim$2 Myr after formation of CAIs with the canonical ^{26}Al/^{27}Al ratio) in the chondrule-forming region with the addition of chondrule-like material.

Relict CAIs inside chondrules clearly formed prior to their host chondrules and experienced reheating during chondrule formation and maybe prior to it as well. This reheating event(s) could have partly or completely reset the ^{26}Al-^{26}Mg systematics of the relict CAIs. As a result, study of the ^{26}Al-^{26}Mg system in relict CAIs in chondrules can potentially provide an age difference between the time of the CAI formation and the time of their reheating during and/or prior to chondrule formation. Although trace element abundances in chondrules (Misawa & Nakamura 1988) and mineralogical observations (e.g., Krot & Keil 2002; Krot et al. 2002a) suggest the presence of CAI-like materials among chondrule precursors, combined mineralogical and O and Mg isotopic studies of relict CAI-bearing chondrules are virtually absent. The only previously reported relict CAI inside a ferromagnesian chondrule is a spinel fragment with inclusions of aluminum-titanium-bearing diopside and nuggets of platinum group elements (PGEs; Misawa & Fujita 1994). The low Al/Mg ratio of the spinel ($\sim$2) in this CAI precluded an Al-Mg isotope study.

In order to understand relative timing of CAI and chondrule formation, we systematically searched for relict CAI-bearing chondrules from a large number of primitive ordinary, enstatite, and carbonaceous chondrites (see § 2) using an X-ray elemental mapping technique. Here, we describe the mineralogy and in situ O and Al-Mg isotope measurements of five relict CAI-bearing chondrules discovered in Acfer 094, Acfer 182, Adelaide, Patuxent Range (PAT) 91546, and Sharps. Acfer 094 (Greshake 1997; Krot et al. 2004a), Acfer 182 (Krot et al. 1999), Adelaide (Krot et al. 2001), and PAT 91546 (Meibom et al. 2000) show no evidence for thermal metamorphism or alteration. Sharps experienced very mild thermal metamorphism and alteration at temperatures of $\sim$330°C $\pm$ 50°C (Brearley 1990).

2. EXPERIMENTAL

X-ray mapping was carried out using a Cameca SX-50 electron microprobe with a 15 kV accelerating voltage, 100 nA beam current, and $\sim$1 μm beam size. X-ray elemental maps in Mg, Ca, Al, and Ti Kα were collected with a resolution of 3–10 μm pixel^{-1} on multiple polished thin sections of the type 3 ordinary (Bishunpur, Krymka, Tieschitz, Semarkona, Sharps), enstatite (EH: ALH A77295, ALH A81189, ALH 88070; EL: QUE 94321), and type 2–3 carbonaceous chondrites (CB: Hammadah al Hamra 237, QUE 94411, QUE 94627; CH: Acfer 182, ALH 85085, EET 96238, PAT 91546, PCA 91238, PCA 91467, RKP 92435; CO: ALH A77307, Y81020, Colony; CR: Acfer 187, El Djouf 001, EET 87730, EET 87770, EET 92042, EET 92174, GRA 95229, MAC 87320, PCA 91082; CV: Efremovka, Leoville, Vigarano; ungrouped: Acfer 094, Adelaide). The search was limited to type 2–3 chondrites, because they largely escaped thermal metamorphism, which could have erased the existing ^{26}Mg* in the CAI and chondrule minerals (LaTourrette & Wasserburg 1997; LaTourrette & Hutcheon 1999). CAI-bearing chondrules were studied using backscattered electron (BSE) imaging, electron probe microanalysis, and an ion microprobe. BSE images were obtained with a JEOL 5900LV scanning electron microscope (SEM) at a 15 kV accelerating voltage and 1–2 nA beam current. Wavelength dispersive element analyses were performed with a Cameca SX-50 electron microprobe at a 15 kV accelerating voltage and 10–20 nA beam current, with a beam size of $\sim$1–2 μm. For each element, counting times on both the peak and background were 30 s (10 s for Na). Matrix effects were corrected by using PAP procedures (Pouchou & Pichoir 1985).

Oxygen isotopic measurements were carried out with the Cameca ims 1270 ion probe at UCLA and with the Cameca ims 6f ion probe at Arizona State University (ASU). Measurements at UCLA were carried out at a high mass resolution with a beam spot size of $\sim$10 μm; for further details see McKeegan et al. (1998). The ^{17}O/^{16}O and ^{18}O/^{16}O ratios are reported as δ^{18}O and δ^{17}O, where $\delta^{17,18}\mathrm{O} = [(^{17,18}\mathrm{O}/^{16}\mathrm{O})_{\mathrm{sample}}/(^{17,18}\mathrm{O}/^{16}\mathrm{O})_{\mathrm{SMOW}} - 1] \times 1000$; SMOW is standard mean ocean water)]. ^{16}O excesses are reported as the deviations in ^{17}O from the terrestrial mass fractionation line: $\Delta^{17}\mathrm{O} = \delta^{17}\mathrm{O} - 0.52\delta^{18}\mathrm{O}$. Instrumental mass fractionation was corrected by using a Burma spinel standard. Under our analytical conditions possible matrix effects between spinel and the Fe-poor minerals analyzed here are <1‰–2‰ amu^{-1} (1 σ). The precision and accuracy for a single analysis of each individual spot is in the range 1‰–2‰ for both δ^{17}O and δ^{18}O.

Oxygen measurements at ASU were carried out using a Cs$^+$ primary ion beam defocused to a spot size of $\sim$20 μm. The ion probe was operated at a mass resolving power of 5500 ($m/\Delta m$) and a 75 eV energy window. The normal-incidence electron flood gun was used for charge compensation. Negative ^{16}O$^-$ ions were measured on the Faraday cup, and ^{17,18}O$^-$ ions were measured on the electron multiplier. Crestmore olivine ($Fa_{0.7}$) was used as the standard. Although there is a large matrix effect associated with FeO content, there does not seem to be a significant matrix effect in FeO-free minerals. The uncertainties reported for the oxygen isotope data come from the statistical uncertainties on each of the measurements, the spread in the standard data ($\pm\sim$2.5 ‰ amu^{-1} [1 σ] in δ^{18}O along the mass fractionation line), and the uncertainty in the detection efficiency factor for multiplier versus Faraday cup.

Aluminum-magnesium ion probe measurements were carried out at UCLA, ASU, and with the Cameca ims 3f ion probe at Lawrence Livermore National Laboratory (LLNL) using standard techniques (Huneke et al. 1983; Fahey et al. 1987). The instruments were operated at a mass resolving power of at least $\sim$2800, sufficient to resolve ^{24}MgH$^+$ from ^{25}Mg$^+$. Instrumental mass fractionation, which differs among the minerals of interest, was accounted for by comparing the measured ^{25}Mg/^{24}Mg ratios for the mineral standards with the ^{25}Mg/^{24}Mg of terrestrial Mg (0.12663; Catanzaro et al. 1966) and is given in parts per thousand (permil, ‰) per amu by

$$\Delta^{25}\mathrm{Mg} = \left[\frac{(^{25}\mathrm{Mg}/^{24}\mathrm{Mg})_{\mathrm{meas}}}{0.12663} - 1\right] \times 1000.$$

Mineral standards were Burma spinel, Madagascar hibonite, chrome diopside, San Carlos olivine, Miakajima plagioclase, and synthetic melilite glass. Excesses or deficits of ^{26}Mg remaining for sample minerals after correcting for instrumental mass fractionation using a linear law (i.e., assuming that the fractionation for ^{26}Mg/^{24}Mg is 2 times that of ^{25}Mg/^{24}Mg) are reported in permil relative to terrestrial Mg (Catanzaro et al. 1966):

$$\delta^{26}\mathrm{Mg} = \left[\frac{(^{26}\mathrm{Mg}/^{24}\mathrm{Mg})_{\mathrm{meas}}}{0.13932} - 1\right] \times 1000.$$

Differences in ionization efficiency between Al and Mg were accounted for by comparing the measured $^{27}Al^+/^{24}Mg^+$ to the "true" $^{27}Al/^{24}Mg$ ratio for each standard mineral. All data are reported with 2 σ uncertainties. Following isotopic analyses, each spot was examined in the scanning electron microscope in backscattered-electron mode to verify the location of the sputtered craters and mineralogical compositions of the phases analyzed.

3. RESULTS

3.1. *Rare Occurrences of Relict CAIs in Ferromagnesian Chondrules*

Relict CAIs within ferromagnesian chondrules are extremely rare. Only five CAI-bearing chondrules were found out of >10,000 chondrules examined. This contrasts with the case for Al-rich chondrules (>10% Al_2O_3 by weight), where >15% contain relict CAIs. Below, we describe the mineralogy, petrography, and O and Mg isotopic compositions of the relict CAIs inside chondrules.

3.2. *Mineralogy and Petrography*

The CAI in chondrule 17 of Acfer 094 (Fig. 1) consists of hibonite surrounded by Fe-rich spinel that is intergrown with chondrule mesostasis. Hibonite and spinel contain tiny inclusions of perovskite, PGE nuggets, and an unidentified Zr-bearing phase. The host chondrule consists of ferrous olivines ($Fa_{33\pm5}$), interstitial anorthitic mesostasis (An_{70-93}), Fe-Cr-spinel, Fe,Ni-sulfides, and rare forsteritic olivines (Fa_4) that are probably relict (Table 1).

The CAI in chondrule 2 of Acfer 182 (Fig. 2) consists of a Mg spinel core surrounded by an anorthite ($An_{99.5}$) layer that is intergrown with chondrule mesostasis. Spinel contains rare inclusions of perovskite. The host chondrule consists of low-Ca pyroxene (Fs_2Wo_5) grains overgrown by high-Ca pyroxene (Fs_2Wo_{40}), Fe,Ni-metal nodules, and fine-grained mesostasis composed of anorthitic plagioclase ($An_{96\pm3}$), high-Ca pyroxene, and a silica phase (Table 1).

The CAI in chondrule 16 of PAT 91546 (Fig. 3) consists of a grossite core surrounded by layers of Mg-spinel and plagioclase that is intergrown with chondrule mesostasis. The host chondrule material consists of forsteritic olivine (Fa_2), low-Ca pyroxene (Fs_2Wo_6), high-Ca pyroxene (Fs_2Wo_{24}), anorthitic mesostasis, and Fe,Ni-metal nodules (Table 1).

The CAI in chondrule 9 of Sharps (Fig. 4*a*), originally described by Bischoff & Keil (1984), consists of hibonite surrounded by Fe-rich spinel and a nepheline-like phase (Table 1). The host chondrule consists of low-Ca pyroxene (Fs_1Wo_4), high-Ca pyroxene (Fs_2Wo_{41}), olivine, glassy mesostasis, and Fe,Ni-metal.

The CAI in chondrule 9d of Adelaide (Fig. 4*b*) consists of hibonite, perovskite, and interstitial melilite, surrounded by a layer of Mg spinel. The host chondrule consists of forsteritic olivine (Fa_1), low-Ca pyroxene (Fs_1Wo_5), anorthitic mesostasis, and Fe,Ni-metal nodules (Table 1). The CAI spinel is corroded by the zone of plagioclase that surrounds the CAI.

3.3. *Oxygen Isotope Compositions*

Oxygen isotopic compositions of chondrules 2, 9d, and 17 and their host CAIs are listed in Table 2 and plotted in Figure 5. We did not measure the O isotopic compositions of the CAIs in chondrules 9 and 16 because these objects are very small, and there is a possibility of contamination by the ^{16}O primary ions used for sputtering during Mg isotope measurements (Aléon et al. 2002).

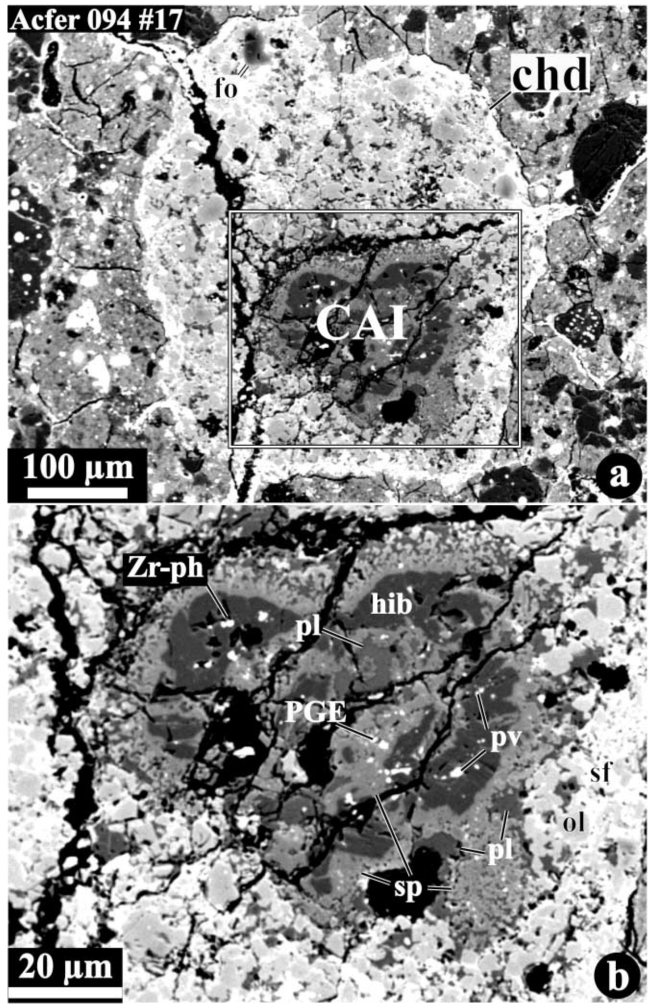

FIG. 1.—BSE images of the CAI-bearing chondrule 17 in the ungrouped carbonaceous chondrite Acfer 094. The relict CAI consists of hibonite (hib) with inclusions of perovskite (pv), a Zr-bearing phase (Zr-ph), and Re,Ir,Os-bearing (PGE) nuggets. It is surrounded by a shell of fine-grained Fe-spinel (sp). The host chondrule consists of ferrous olivine (ol), plagioclase mesostasis (pl), Fe,Ni-sulfides (sf), Cr-spinel, and relict grains of forsteritic olivine (fo). The region outlined in (*a*) is shown in detail in (*b*).

Spinel in CAI 2 from Acfer 182 is enriched in ^{16}O ($\Delta^{17}O \sim -20‰$) relative to plagioclase ($\Delta^{17}O \sim -8‰$). Pyroxenes in the surrounding chondrule are ^{16}O-poor ($\Delta^{17}O \sim -1‰$).

Hibonite in CAI 17 from Acfer 094 is enriched in ^{16}O ($\Delta^{17}O = -20‰$ to $-23‰$). The spinel analyses are relatively ^{16}O-poor ($\Delta^{17}O = -6‰$ to $-17‰$), probably due to overlap of the beam onto plagioclase mesostasis ($\Delta^{17}O = -3.3‰$ to $-5.1‰$) in the adjacent chondrule. Within the chondrule, a relict forsterite grain is more ^{16}O enriched ($\Delta^{17}O = -4.4‰$) than the fayalitic olivines ($\Delta^{17}O = -3.2‰$ to $-0.6‰$).

Hibonite and melilite in CAI 9d from Adelaide were too small to measure individually with the $\sim$20 μm primary beam. However, mixtures of the two minerals are very ^{16}O-rich ($\Delta^{17}O \sim -23‰$). Chondrule olivines and plagioclase are much less ^{16}O-rich ($\Delta^{17}O = -6‰$ to $-9‰$).

3.4. *Aluminum-Magnesium Isotope Compositions*

Magnesium isotope compositions of the CAIs and host chondrules are listed in Table 3 and plotted in Figure 6.

None of the minerals in Acfer 094 CAI 17 or its host chondrule show any $^{26}Mg^*$. The upper limit on $(^{26}Al/^{27}Al)_I$ inferred

TABLE 1

Electron Microprobe Analyses (in Percent by Weight) of Minerals in Relict Ca-Al-rich Inclusions and Host Chondrules

CAI or Chondrule	Mineral	SiO_2	TiO_2	Al_2O_3	Cr_2O_3	FeO	MnO	MgO	CaO	Na_2O	K_2O	Total
Acfer 094												
CAI 17	hib	<0.03	1.6	88.8	<0.03	0.28	<0.07	0.80	8.6	<0.05	<0.04	100.1
	sp	0.38	0.73	63.2	0.27	20.0	0.15	14.4	0.23	<0.05	<0.04	99.3
Chd. 17	plag	44.4	0.16	35.3	<0.03	0.56	<0.07	0.07	18.9	0.74	<0.04	100.2
	plag	50.1	0.08	31.0	<0.03	0.99	<0.07	0.19	14.3	3.4	<0.04	100.1
	ol	42	0.11	0.06	0.30	4.5	0.11	54.4	0.24	<0.05	<0.04	101.6
	ol	36.6	0.03	0.11	0.17	29.0	0.31	33.2	0.5	<0.05	<0.04	100
Acfer 182												
CAI 2	sp	0.09	1.1	69.5	0.61	1.6	0.20	26.8	0.09	<0.05	<0.04	100.1
	plag	42.6	0.15	36.4	0.10	0.29	<0.07	0.27	19.9	<0.05	<0.04	99.7
Chd. 2	plag	45.6	0.12	34.0	<0.03	0.33	<0.07	0.61	18.9	0.45	<0.04	100.1
	sil	96.6	0.31	0.99	<0.03	0.52	<0.07	0.15	0.50	0.16	<0.04	99.3
	px	57.4	0.54	1.3	1.0	1.6	0.29	35.5	2.7	<0.05	<0.04	100.3
	px	52.1	2.3	3.0	1.4	1.1	0.56	20.0	18.9	<0.05	<0.04	99.4
PAT 91546												
CAI 16	grs	0.11	0.38	77.4	0.04	0.68	<0.03	<0.03	21.5	<0.05	<0.04	100.1
Chd. 16	px	57.1	0.17	2.0	0.79	1.7	0.13	36.5	3.1	<0.05	<0.04	101.5
	px	54.7	0.37	2.3	0.75	1.9	0.12	27.5	13.2	<0.05	<0.04	100.9
	ol	42.2	<0.03	0.04	0.53	2.4	0.14	55.6	0.28	<0.05	<0.04	101.2
	plag	43.4	<0.03	32.61	0.08	2.1	<0.07	1.2	18.9	<0.05	<0.04	98.3
Adelaide												
CAI 9d	hib	1.4	2.3	86.2	0.05	0.21	<0.07	1.3	9.4	<0.05	<0.04	100.9
	sp	0.13	0.56	72.5	0.41	0.88	<0.07	27.1	0.09	<0.05	<0.04	101.7
Chd. 9d	ol	42.7	0.07	<0.05	0.56	0.63	0.19	56.3	0.22	<0.05	<0.04	100.7
	px	57.9	0.43	1.7	0.54	0.57	0.16	36.7	2.7	<0.05	<0.04	100.8
	mes	41.7	<0.04	34.0	<0.04	3.73	<0.07	0.7	16.8	0.88	<0.04	97.8
	mes	46.3	0.23	28.6	0.13	0.97	<0.07	8.3	15.9	0.65	<0.04	101.1
	mes	38.7	0.36	39.2	0.27	0.39	<0.07	2.6	18.0	0.26	<0.04	99.9
Sharps												
CAI 9	hib	0.20	1.8	87.4	n.a.	0.92	n.a.	0.95	8.4	0.09	n.a.	99.8
	nph	43.0	<0.06	35.7	n.a.	0.72	n.a.	0.12	1.4	16.1	n.a.	97.0
	sp	<0.03	0.54	64.6	<0.04	22.3	<0.07	12.2	0.26	n.a.	n.a.	99.9
Chd. 9	ol	42.4	<0.06	<0.05	<0.11	4.6	0.12	52.4	0.25	n.a.	n.a.	99.8
	px	58.8	0.49	0.89	0.38	0.73	<0.07	36.7	2.0	n.a.	n.a.	100.0
	px	54.3	1.1	2.8	0.17	1.3	0.15	20.1	20.0	n.a.	n.a.	99.9

Note.—Grs, grossite; hib, hibonite; nph, nepheline, ol, olivine; plag, plagioclase; px, pyroxene; sil, silica; sp, spinel; and n.a., not analyzed.

from these data for this compound object is 1×10^{-5} (Fig. 6*a*). The δ^{26}Mg values for hibonite in the CAI and for mixtures of hibonite and plagioclase are negative, averaging $\sim -3.3‰ \pm 0.9‰$ (Table 2). Negative δ^{26}Mg values are unusual, but have been observed in hibonite-bearing microspherules (Ireland et al. 1991; Simon et al. 1997; Russell et al. 1998) and in some FUN (fractionation and unknown nuclear anomalies) CAIs from CV meteorites (Lee & Papanastassiou 1974; Clayton et al. 1984). It is impossible to determine from our data whether the anomalies represent true deficits of ^{26}Mg, or excesses of ^{25}Mg or deficits of ^{24}Mg (which translate into ^{26}Mg deficits because of the correction for instrumental mass fractionation). However, one interpretation is that CAI 17 formed from a reservoir that was deficient in ^{26}Mg and did not acquire any ^{26}Al. The Fe-rich spinel, which is probably a secondary phase in CAI 17, shows no anomaly in ^{26}Mg.

Plagioclase in Acfer 182 CAI 2 and in the host chondrule shows no resolved ^{26}Mg*. The upper limits on $(^{26}Al/^{27}Al)_I$ in the CAI and chondrule are 6×10^{-6} and 4×10^{-6}, respectively (Fig. 6*b*). Similarly, hibonite and nepheline in Sharps CAI 9 show no evidence of ^{26}Mg* and give an upper limit on $(^{26}Al/^{27}Al)_I$ of 1.3×10^{-5} (Fig. 6*b*).

Grossite in PAT 91546 CAI 16 shows a resolved excess of ^{26}Mg. If this excess is assumed to be radiogenic and the underlying Mg is assumed to have a normal $^{26}Mg/^{24}Mg$ ratio, then a model isochron gives an $(^{26}Al/^{27}Al)_I$ of $(1.7 \pm 1.3) \times 10^{-6}$ (Fig. 6*c*).

Hibonite in Adelaide CAI 9d shows clear excesses of radiogenic ^{26}Mg correlated with $^{27}Al/^{24}Mg$, and together with spinel forms an isochron giving an $(^{26}Al/^{27}Al)_I$ of $(3.7 \pm 0.5) \times 10^{-5}$ (Fig. 6*d*). The cleanest (based on Si count rate) measurement of melilite in CAI 9d shows no ^{26}Mg*, while a mixture of hibonite and melilite shows an intermediate ^{26}Mg excess that appears to plot on a mixing line connecting melilite and the most ^{26}Mg*-enriched hibonite. Two measurements of plagioclase in the host

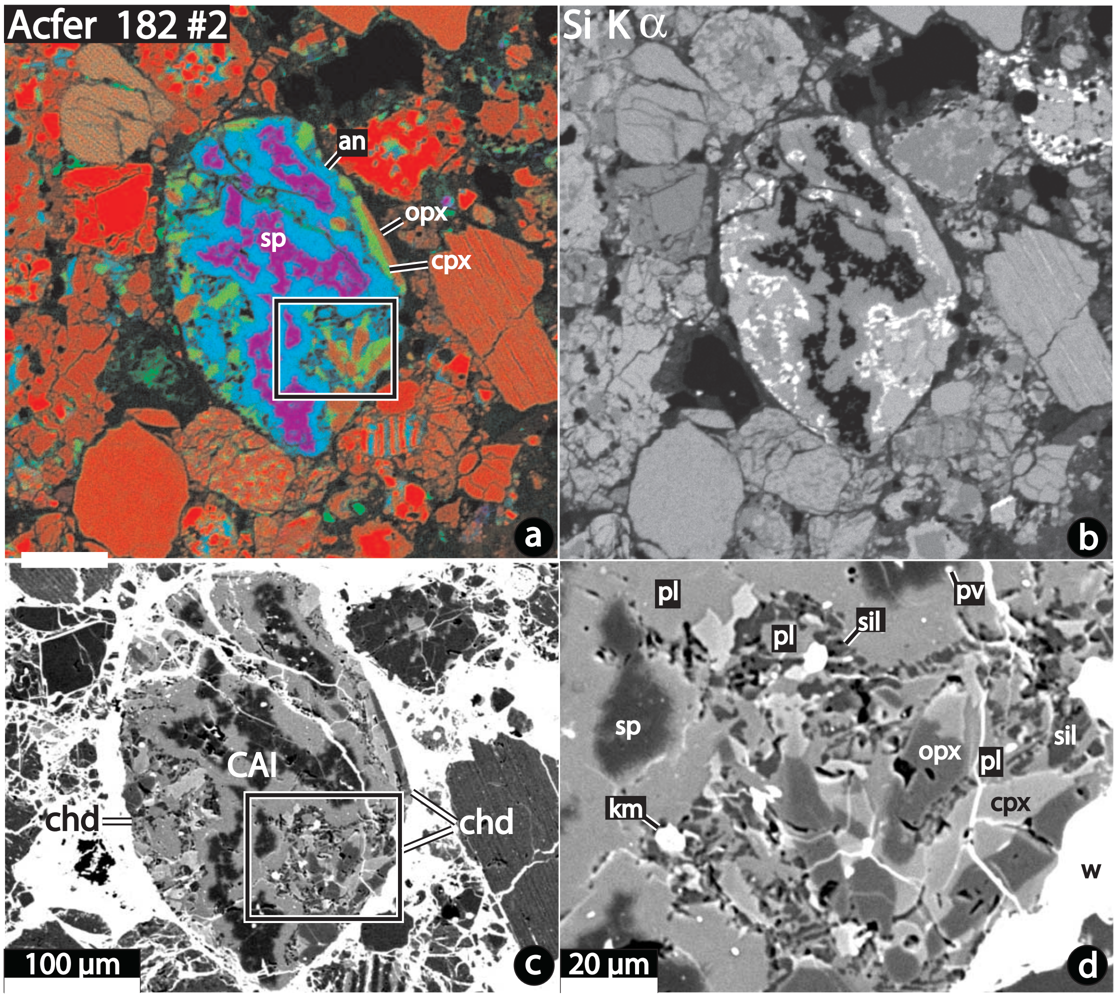

Fig. 2.—(*a*) Combined elemental map in Mg (*red*), Ca (*green*), and Al Kα (*blue*) X-rays, (*b*) elemental map in Si Kα X-rays, and (*c*, *d*) BSE images of the CAI-bearing chondrule 2 in the CH carbonaceous chondrite Acfer 182. The relict CAI consists of Mg-spinel (sp) surrounded by an anorthite (an) rim; perovskite (pv) is minor. The host chondrule consists of low-Ca pyroxene (opx), high-Ca pyroxene (cpx), and fine-grained mesostasis composed of silica (sil), anorthite, high-Ca pyroxene, and kamacitic metal (km). The region outlined in (*a*) and (*c*) is shown in detail in (*d*).

chondrule, which were made in the rim around the CAI, show no resolvable ^{26}Mg* [$(^{26}\mathrm{Al}/^{27}\mathrm{Al})_I < 5 \times 10^{-6}$].

4. DISCUSSION

4.1. *The Rarity of Relict CAIs in Ferromagnesian Chondrules*

Relict CAIs are extremely rare in ferromagnesian chondrules (only five have been found so far), but are common in the Al-rich (>10% Al_2O_3 by weight) chondrules (>15% of them contain relict CAIs). These observations suggest a close genetic relationship between the CAIs and Al-rich chondrules: many of the latter appear to have formed by melting of CAIs mixed with ferromagnesian chondrule precursors (Krot & Keil 2002; Krot et al. 2001, 2002a, 2004a). At the same time, the vast majority of CAIs outside of chondrules do not show clear mineralogical evidence for being affected by chondrule melting. For example, (1) many CAIs are irregularly shaped and porous and show no evidence for being melted. (2) Both igneous and nonigneous CAIs outside of chondrules are surrounded by multilayered ^{16}O-rich Wark-Lovering rims,[11] which are believed to have formed by evaporation-condensation processes in an ^{16}O-rich gaseous reservoir, in the CAI-forming region (Krot et al. 2002b). If CAIs were melted during chondrule formation, one could expect that (*a*) the Wark-Lovering rims would have been partly or completely destroyed (depends on the degree of melting), and (*b*) these rims would have experienced O isotopic exchange with an ^{16}O-poor gas, typical for the chondrule-forming regions (Leshin et al. 1998; Krot et al. 2004b, 2005b). Neither of these features has been observed yet. (3) In addition, coarse-grained igneous (type B and compact type A) CAIs in CV carbonaceous chondrites are often surrounded by forsterite-rich accretionary rims, which are enriched in ^{16}O to a level similar to that observed in the most ^{16}O-rich primary CAI minerals, suggesting that these CAIs were melted in the CAI-forming regions (Krot et al. 2002b, 2005b). These observations suggest that either CAIs outside of chondrules were largely absent from the chondrule-forming regions at the time of chondrule formation or, which is probably more likely, chondrule-forming events in a specific nebular region were highly localized.

4.2. *Nature and Relationships of the CAIs and Chondrules*

The microporphyritic textures of the CAI-bearing chondrules, the presence of igneously zoned pyroxene grains, the presence of rounded Fe,Ni-metal nodules and glassy or fine-grained

[11] The Wark-Lovering rim sequence around CAIs outside chondrules consists of ±spinel, ±melilite, ±anorthite, diopside, and ±forsterite; diopside or forsterite are the outermost layers and are believed to have formed by gas-solid condensation (Wark & Lovering 1977).

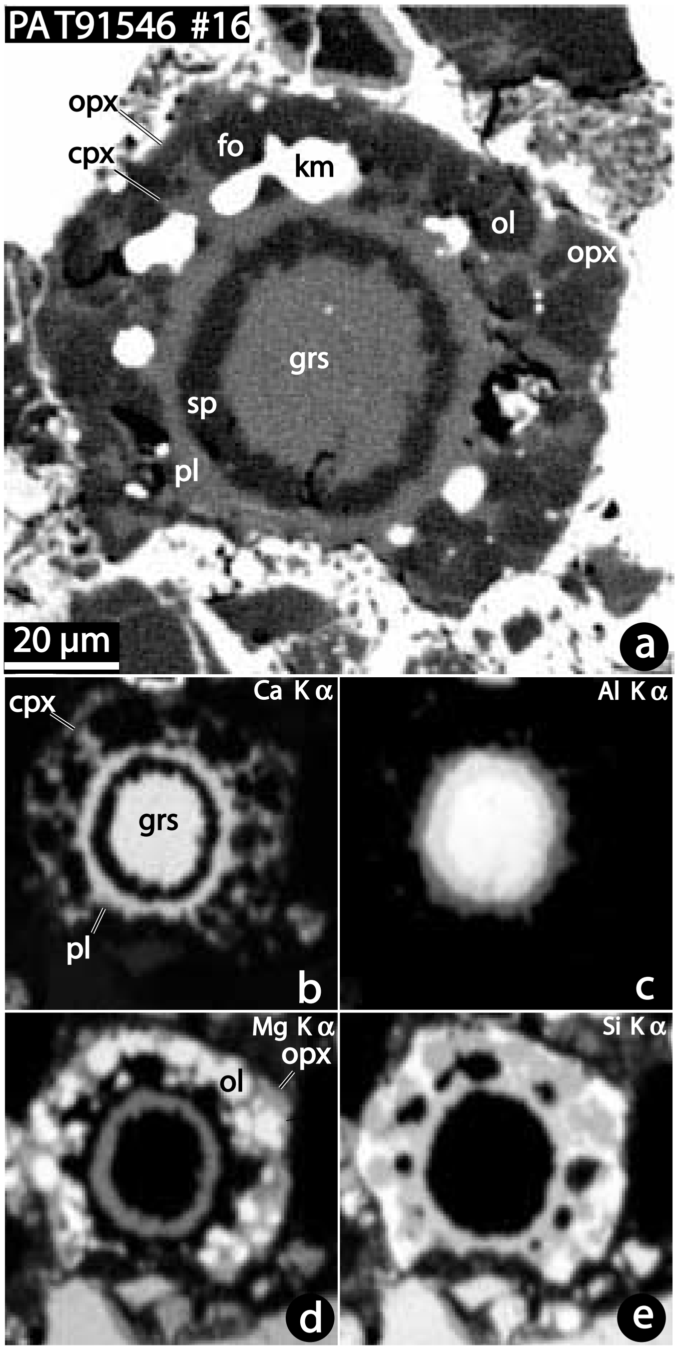

FIG. 3.—(*a*) BSE image and elemental maps in (*b*) Ca, (*c*) Al, (*d*) Mg, and (*e*) Si Kα X-rays of the CAI-bearing chondrule 16 in the CH carbonaceous chondrite PAT 91546. The relict CAI consists of grossite (grs) surrounded by a Mg-spinel (sp) rim. The host chondrule consists of forsteritic olivine (fo), low-Ca pyroxene (opx), high-Ca pyroxene (cpx), anorthitic mesostasis (pl), and kamacitic metal (km).

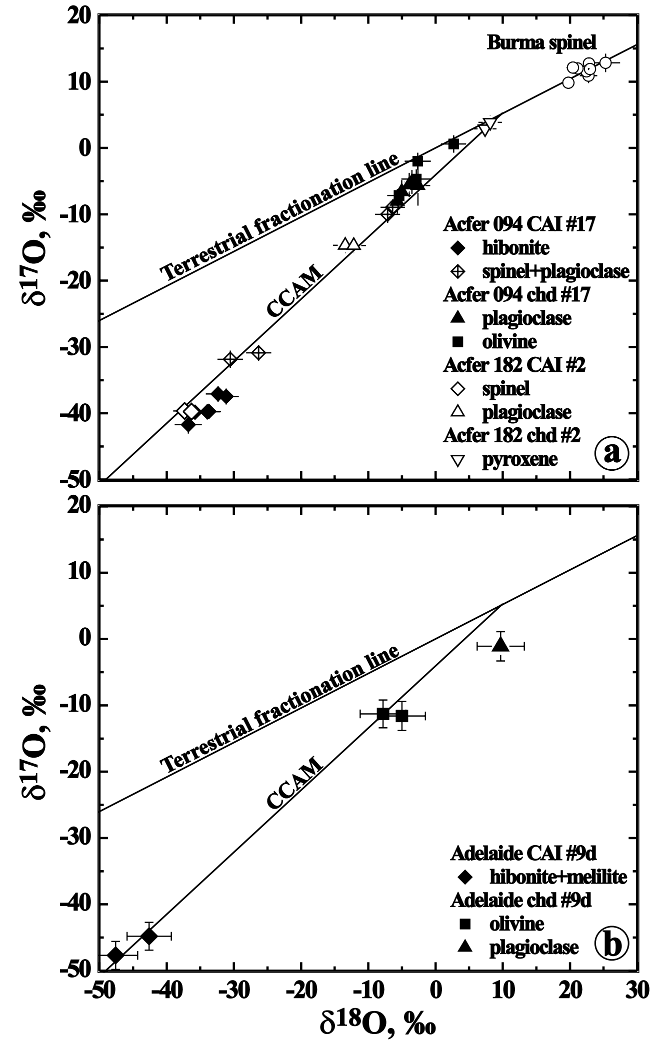

FIG. 4.—BSE images of the CAI-bearing chondrules (*a*) 9 in the H3.4 ordinary chondrite Sharps, and (*b*) 9d in the ungrouped carbonaceous chondrite Adelaide. The relict CAI in (*a*), Sharps, consists of a nepheline-like phase (nph), hibonite (hib), and Fe-spinel (sp). The host chondrule consists of forsteritic olivine (ol), low-Ca pyroxene (opx), high-Ca pyroxene (cpx), anorthitic mesostasis (mes), and kamacitic metal (km). The relict CAI in (*b*), Adelaide, consists of hibonite (hib), perovskite (pv), and melilite (mel); it is surrounded by a Mg-spinel (sp) rim. The host chondrule consists of forsteritic olivine (ol), low-Ca pyroxene (px), glassy mesostasis (pl), and kamacitic metal (km).

mesostasis, and the presence of relict forsteritic olivine overgrown by fayalitic olivine indicate that these chondrules crystallized from melts. The refractory mineralogies of the CAIs, which are out of equilibrium with the chondrule melts, and the ^{16}O enrichment of spinel and hibonite in CAIs 2, 17, and 9d relative to their host chondrules indicate that the CAIs predate the chondrules and are relict. The observed intergrowths between the chondrule mesostases and spinel or anorthite of the relict CAIs, and the absence of a complete Wark-Lovering rim sequence around the CAIs, indicate that they have been partly melted and corroded by chondrule melts. This interpretation is supported by the ^{16}O depletion of anorthite compared to spinel in the CAI 2, which probably resulted from O isotopic exchange between the CAI anorthite and the chondrule melt (Fig. 5*a*).

Because CAIs in chondrules are so rare, it is important to consider whether the relict CAIs are representative of the CAIs that are common constituents of many types of chondrites. Adelaide CAI 9d is a hibonite-melilite-spinel object (Fig. 4*b*) that was originally very ^{16}O-rich and formed with a high $(^{26}\mathrm{Al}/^{27}\mathrm{Al})_I$ ratio of $(3.7 \pm 0.5) \times 10^{-5}$. These characteristics are completely consistent with "normal" CAIs in Adelaide and other meteorites (Krot et al. 2001; Huss et al. 2002).

PAT 91546 CAI 16 consists of grossite surrounded by a layer of spinel. Grossite shows an excess of ^{26}Mg, although the $(^{26}\mathrm{Al}/^{27}\mathrm{Al})_I$ ratio of $(1.7 \pm 1.3) \times 10^{-6}$ is much lower than the "canonical" value of 5×10^{-5} common in "normal" CAIs. Although CAIs with the canonical $(^{26}\mathrm{Al}/^{27}\mathrm{Al})_I$ ratio have also been described in CH chondrites, most of the grossite-rich CAIs in CHs either contain no radiogenic ^{26}Mg or have small $^{26}\mathrm{Al}/^{27}\mathrm{Al}$

TABLE 2

Oxygen Isotopic Compositions of Minerals in the Relict CAIs and Host Chondrules from the Acfer 094, Acfer 182, and Adelaide Chondrites

Mineral	$\delta^{18}O$ (‰)	$\delta^{17}O$ (‰)	$\Delta^{17}O$ (‰)
Acfer 094 CAI 17			
hib 1	−36.8 ± 2.0	−41.7 ± 1.4	−22.6 ± 2.4
hib 2	−34.0 ± 1.9	−39.8 ± 1.2	−22.1 ± 2.3
hib 3	−35.8 ± 1.7	−39.8 ± 1.1	−21.2 ± 2.1
hib 4	−33.7 ± 1.8	−39.7 ± 1.1	−22.2 ± 2.1
hib 5	−31.1 ± 1.9	−37.5 ± 1.2	−21.3 ± 2.2
hib 6	−32.4 ± 1.8	−37.1 ± 1.2	−20.3 ± 2.2
sp + plag 1	−30.5 ± 1.9	−31.8 ± 1.3	−16.0 ± 2.3
sp + plag 2	−26.3 ± 1.9	−30.9 ± 1.2	−17.2 ± 2.2
sp + plag 3	−7.1 ± 1.9	−10.0 ± 1.3	−6.3 ± 2.3
sp + plag 4	−6.4 ± 1.8	−8.9 ± 1.2	−5.6 ± 2.2
Acfer 094 Chondrule 17			
fa 1	2.7 ± 1.9	0.6 ± 1.3	−0.8 ± 2.3
fa 2	−2.9 ± 2.3	−4.7 ± 1.5	−3.2 ± 2.7
fa 3	−2.7 ± 1.9	−2.0 ± 1.3	−0.6 ± 2.3
fo	−5.4 ± 1.8	−7.2 ± 1.2	−4.4 ± 2.1
plag 1	−5.7 ± 1.9	−8.1 ± 1.1	−5.1 ± 2.2
plag 2	−5.0 ± 1.7	−6.6 ± 1.2	−4.0 ± 2.1
plag 3	−2.6 ± 3.0	−5.7 ± 1.8	−4.3 ± 3.5
plag 4	−3.9 ± 1.8	−5.6 ± 1.2	−3.5 ± 2.1
plag 5	−3.5 ± 1.8	−5.1 ± 1.1	−3.3 ± 2.1
Acfer 182 CAI 2			
sp 1	−37.3 ± 1.7	−39.7 ± 1.0	−20.2 ± 2.0
sp 2	−36.3 ± 1.7	−39.7 ± 1.0	−20.8 ± 2.0
plag 1	−13.4 ± 1.8	−14.7 ± 1.1	−7.7 ± 2.1
plag 2	−12.2 ± 1.8	−14.7 ± 1.1	−8.4 ± 2.1
Acfer 182 Chondrule 2			
px 1	7.4 ± 1.7	2.9 ± 1.0	−1.0 ± 2.0
px 2	8.1 ± 1.7	3.9 ± 1.1	−0.4 ± 2.0
Adelaide CAI 9d			
hib + mel 1	−47.6 ± 3.3	−47.7 ± 2.1	−23.0 ± 3.9
hib + mel 2	−42.6 ± 3.3	−44.8 ± 2.1	−22.6 ± 3.9
Adelaide Chondrule 9d			
fo 1	−7.8 ± 3.4	−11.3 ± 2.1	−7.3 ± 4.0
fo 2	−5.0 ± 3.5	−11.6 ± 2.2	−9.0 ± 4.1
plag	9.7 ± 3.5	−1.1 ± 2.2	−6.1 ± 4.2

Notes.—Errors are 1 σ. Fa, fayaltitic olivine; fo, forsteritic olivine; hib, hibonite; mel, melilite; plag, plagioclase; px, high-Ca pyroxene; and sp, spinel.

ratios (MacPherson et al. 1989; Kimura et al. 1993; Weber et al. 1995). As a result, we cannot exclude the possibility that CAI 16 initially contained a low abundance of ^{26}Al.

Sharps CAI 9 currently consists of hibonite and nepheline surrounded by a layer of Fe-rich spinel (Fig. 4*a*). Nepheline often replaces melilite in CAIs from CV3 chondrites, and spinel can become Fe-rich by metasomatism or by exchange with the surrounding chondrule (MacPherson et al. 1988). An original mineralogy of hibonite, melilite, and Mg-spinel would be quite consistent with a "normal" CAI. However, the hibonite in CAI 9 does not show any evidence of ^{26}Al. Hibonite apparently remains closed to Mg diffusion to higher temperatures than other CAI minerals (e.g., Russell et al. 1998; Adelaide CAI 9d). Thus, it is unclear whether Sharps CAI 9 has had its ^{26}Al clock reset prior to or during chondrule melting in the solar nebula or during thermal metamorphism and alteration on the Sharps parent asteroid, or never had any ^{26}Al.

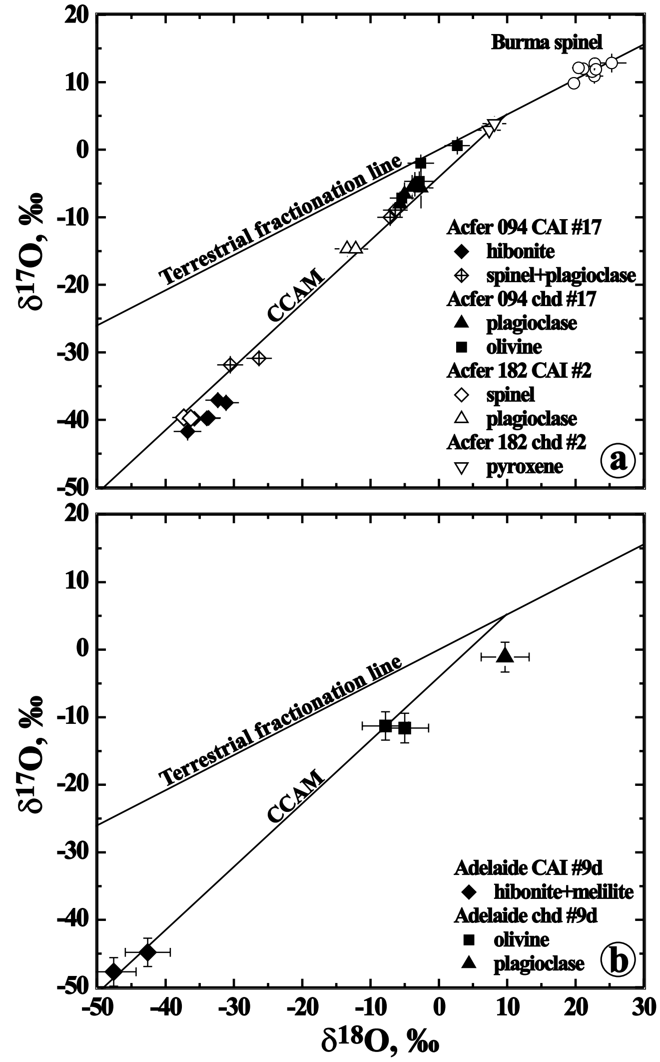

Fig. 5.—Oxygen isotopic compositions of individual minerals in the relict CAI-bearing chondrules 17 in Acfer 094, 2 in Acfer 182, and 9d in Adelaide. The terrestrial fractionation line and carbonaceous chondrite anhydrous mineral (CCAM) line are shown for reference.

Acfer 182 CAI 2 is currently composed of ^{16}O-rich spinel surrounded by plagioclase, with minor perovskite. The plagioclase is probably a reaction product between melilite and SiO gas, as commonly observed in fine-grained, spinel-rich CAIs in primitive chondrites (e.g., Lin & Kimura 1998; Krot et al. 2004c). However, plagioclase is much less ^{16}O-rich than the coexisting spinel, suggesting that it must have experienced melting and O isotope exchange during chondrule formation (Krot et al. 2004b, 2005b). This melting could have resulted in resetting of the Al-Mg system in plagioclase (spinel is too Mg-rich to see an ^{26}Al effect).

All of these CAIs have characteristics that are consistent with the hypothesis that they formed as "normal" CAIs that were later captured by chondrules.

An exception to this may be CAI 17 from Acfer 094. This CAI currently consists of hibonite surrounded by a layer of Fe-rich spinel intergrown with chondrule(?) plagioclase. This mineralogy is consistent with an original CAI consisting of hibonite, Mg spinel, and melilite surrounded by a Wark-Lovering rim sequence.

TABLE 3

Aluminum-Magnesium Isotopic Data for Relict CAIs and Host Chondrules in Acfer 094, Acfer 182, Adelaide, PAT 91546, and Sharps

Mineral	δ^{26}Mg (‰)	^{27}Al/^{24}Mg
Acfer 094 CAI 17		
hib 1	−2.6 ± 1.3	13.0 ± 1.3
hib 2	−1.8 ± 3.3	57.0 ± 5.7
hib 3	−5.2 ± 2.0	93.4 ± 9.3
sp	1.1 ± 1.3	4.4 ± 0.4
hib + plag 1	−2.9 ± 2.8	122.2 ± 12.2
hib + plag 2	−4.2 ± 2.6	119.8 ± 12.0
Acfer 094 Chondrule 17		
plag	1.2 ± 6.8	111.1 ± 11.1
ol 1	0.4 ± 1.0	<0.01
ol 2	−0.5 ± 1.7	<0.01
ol 3	−0.4 ± 1.8	<0.01
ol 4	0.8 ± 0.9	<0.01
Acfer 182 CAI 2		
plag 1	−1.5 ± 4.3	65.5 ± 6.5
plag 2	3.2 ± 2.2	140.2 ± 14.0
plag 3	0.0 ± 1.6	38.2 ± 3.8
sp	−0.6 ± 2.1	2.6 ± 0.3
Acfer 182 Chondrule 2		
plag	−0.2 ± 1.1	35.4 ± 3.5
Adelaide CAI 9d		
hib 1	24.0 ± 1.9	95.3 ± 4.8
hib 2	13.7 ± 4.2	57.2 ± 2.9
hib 3	18.5 ± 5.9	81.2 ± 4.1
hib-mel mix 1	8.4 ± 5.6	46.9 ± 2.5
hib-mel mix 2	−0.4 ± 3.7	17.3 ± 1.0
sp 1	−0.7 ± 2.8	2.7 ± 0.1
sp 2	−0.6 ± 2.5	3.4 ± 0.2
Adelaide Chondrule 9d		
plag 1	−3.7 ± 3.2	66.4 ± 3.4
plag 2	−1.3 ± 5.0	42.2 ± 2.4
ol 1	0.1 ± 2.3	0.015 ± 0.008
ol 2	−0.5 ± 2.3	0.014 ± 0.002
PAT 91546 CAI 16		
grs	23.0 ± 16.0	1900.0 ± 110.0
PAT 91546 Chondrule 16		
ol	0.4 ± 1.0	<0.01
Sharps CAI 9		
hib 1	2.3 ± 2.5	7.7 ± 0.4
hib 2	0.0 ± 4.6	19.3 ± 0.6
hib 3	0.1 ± 4.3	38.5 ± 0.3
nph	−2.6 ± 5.0	12.2 ± 0.1
Sharps Chondrule 9		
ol	−0.6 ± 1.1	<0.01

Notes.—Errors are 2 $\sigma_{\rm mean}$. Grs, grossite; hib, hibonite; mel, melilite; ol, olivine; plag, plagioclase; and sp, spinel.

The oxygen isotopes of hibonite and spinel + plagioclase are ^{16}O-rich, but instead of showing evidence of radiogenic ^{26}Mg*, the δ^{26}Mg values for hibonite are negative, showing an apparent ∼3‰ deficit of ^{26}Mg. Although CAIs exhibiting deficits of ^{26}Mg have been previously observed (Lee & Papanastassiou 1974; Clayton et al. 1984; Ireland et al. 1991; Simon et al. 1997; Russell et al. 1998), they are not common and are thought by many to have formed in a separate environment from normal CAIs. However, an unusual inclusion can appear in any population, so perhaps this is simply the "exception that proves the rule," and the CAIs we observed inside chondrules are representative of the broader population of CAIs.

4.3. *Chronological Information*

The most convincing chronological interpretation can be made for Adelaide CAI 9d and its surrounding chondrule. The CAI, which is ^{16}O-rich and has a mineralogy similar to many "normal" CAIs, apparently formed with a high $(^{26}\mathrm{Al}/^{27}\mathrm{Al})_I$ ratio of $(3.7 \pm 0.5) \times 10^{-5}$, close to the canonical $(^{26}\mathrm{Al}/^{27}\mathrm{Al})_I$ for the early solar system. Evidence of this high ratio is preserved in hibonite, a phase that is resistant to thermal redistribution of Mg isotopes (e.g., Russell et al. 1998). When CAI 9d was incorporated into the surrounding chondrule melt, diopside, melilite (or anorthite), and spinel of its Wark-Lovering rim sequence began reacting with the surrounding chondrule melt to produce a layer of plagioclase, and melilite in the interior of the inclusion exchanged Mg with the surrounding chondrule melt. The newly formed plagioclase and the melilite inside the CAI no longer contain evidence of ^{26}Mg*. This constrains the timing of the chondrule melting event to be at least 2 Myr after the CAI formed, because >80% of ^{26}Al had decayed. Thus, Adelaide CAI 9d and its surrounding chondrule provide clear evidence of a ≥2 Myr time gap between the formation of the CAI and its incorporation into the chondrule, and this evidence does not contain an assumption of a homogeneous distribution of ^{26}Al in the chondrule-forming region (MacPherson et al. 1995).

The petrography, O isotopes, and Al-Mg systematics of PAT 91546 CAI 16, Acfer 182 CAI 2, and Sharps CAI 9 can be interpreted in a similar way. If we assume that these objects formed with the canonical CAI $(^{26}\mathrm{Al}/^{27}\mathrm{Al})_I$ ratio of 5×10^{-5}, then for a melting event to reduce the inferred $(^{26}\mathrm{Al}/^{27}\mathrm{Al})_I$ ratio by a factor of 28 (PAT 91546 CAI 16) or more, that melting event must have taken place ≥3 Myr after the CAI formed. Another possibility, that evidence of ^{26}Al was destroyed by parent-body metamorphism after accretion, can probably be excluded for Acfer 094 and Acfer 182, which escaped thermal metamorphism (Greshake 1997; Krot et al. 1999). However, Sharps experienced mild thermal metamorphism (Brearley 1990) and hydrothermal alteration (Krot & Wasson 1994), which may have erased evidence of ^{26}Mg* in hibonite.

Of course, there is a viable alternate interpretation for PAT 91546 CAI 16, Acfer 182 CAI 2, and Sharps CAI 9. They could have formed initially with very little (CAI 16) or no ^{26}Al (CAI 2, CAI 9; see, e.g., MacPherson et al. 1989; Kimura et al. 1993; Weber et al. 1995). If so, then the chondrule melting event did not reset the ^{26}Al clock, and there would be no chronological information, besides that the relict CAIs predate formation of the host chondrules. Acfer 094 CAI 17, which has an apparent deficit in ^{26}Mg (Table 1), shows evidence of never having contained ^{26}Al. In this case, it is clear that no information about the timing of the chondrule melting event can be obtained.

The observed difference in O isotopic compositions of the relict CAIs (^{16}O-rich) and the host chondrules (^{16}O-poor) is also consistent with the earlier formation of the CAIs. The currently

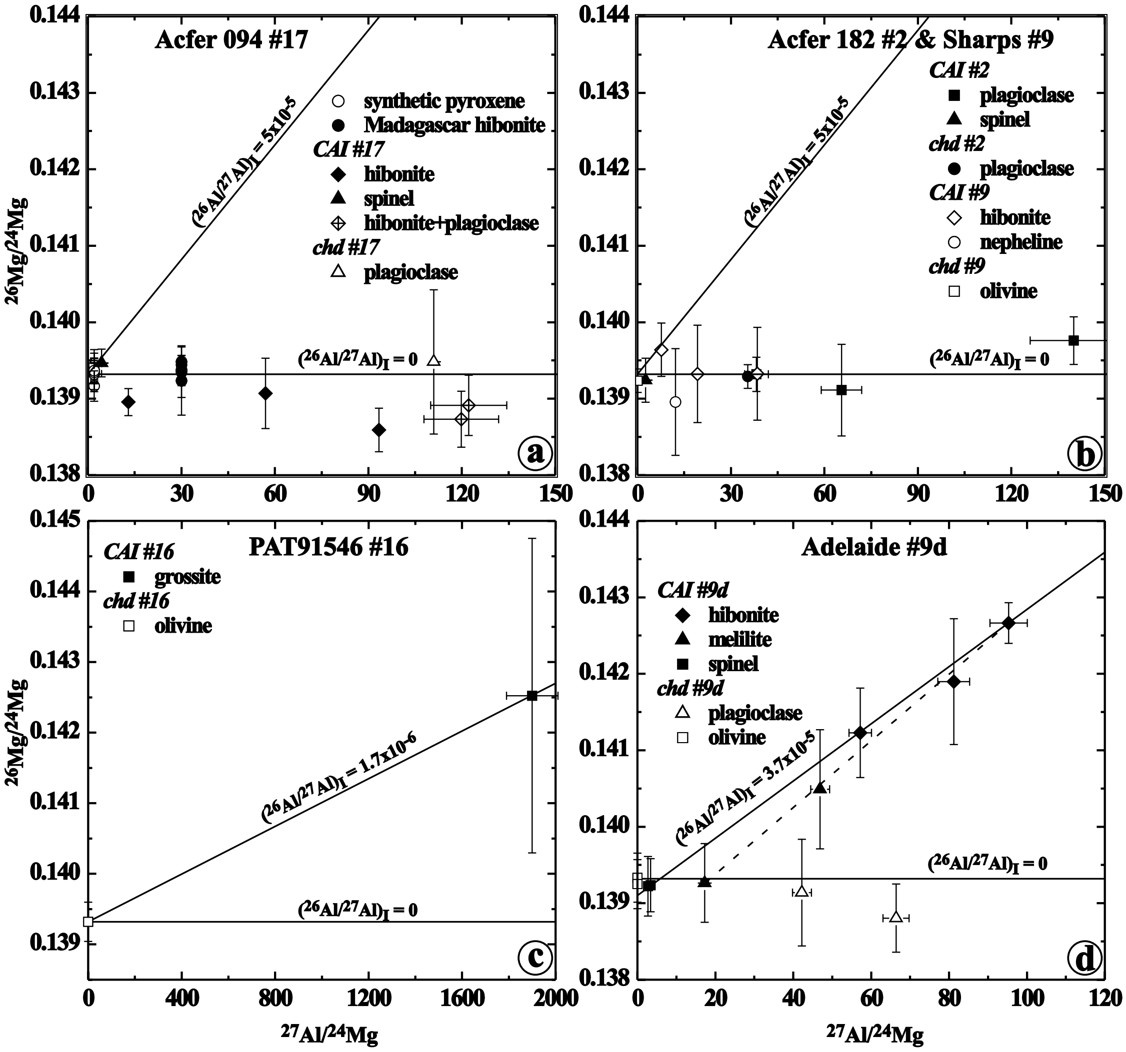

FIG. 6.—Aluminum-magnesium evolution diagrams for relict CAIs and host chondrules (*a*) 17 in Acfer 094, (*b*) 2 in Acfer 182 and 9 in Sharps, (*c*) 16 in PAT 91546, and (*d*) 9d in Adelaide.

favored model of the origin of the ^{16}O anomaly and evolution of the O isotopic composition in the inner solar nebula is based on CO self-shielding (Clayton 2002; Yurimoto & Kuramoto 2004; Krot et al. 2005b; Lyons & Young 2005; Hashizume & Chaussidon 2005). According to this model, the nebular gas was initially ^{16}O-rich. During this time ^{16}O-rich CAIs formed. A later influx of ^{17,18}O-rich water from the outer solar system, produced through the self-shielding mechanism, caused the inner solar nebula to become ^{16}O depleted (e.g., Cuzzi & Zahnle 2004). Chondrules formed during this stage.

In summary, we have one clear case, Adelaide CAI 9d, that shows that chondrule melting took place $\geq$2 Myr after the CAI formed and one clear case where the CAI formed without any ^{26}Al. The other three CAIs have mineralogies and, in the one case where we could measure them, O isotopes consistent with "normal" CAIs. The ^{26}Al and O isotopic data independently indicate that the CAIs formed early and were incorporated into chondrules after several Myr.

4.4. *Broader Implications*

The inferred 2–3 Myr age difference between formation of the relict CAIs and that of their host chondrules has implications for the locations of chondrule and CAI formation. There are two main models, the jet-flow model and shock model (e.g., Jones et al. 2000). In the jet-flow model, chondrules and CAIs formed close to the Sun, in the region where the Sun's magnetosphere interacts with the solar nebula to form a high-speed jet that flows perpendicular to the disk (Liffman 1992; Liffman & Brown 1996; Shu et al. 1996, 2001). The jet flow ejects CAIs and chondrules to the outer parts of the nebula, where they may aggregate to form chondrites. The shock model assumes that shock waves occurred in the solar nebula at $\sim$2–3 AU from the Sun and converted dust balls into chondrules and CAIs (Iida et al. 2001; Desch & Connolly 2002). The source of the shock waves remains unknown; proposed mechanisms include spiral density waves (Wood 1996; Desch & Connolly 2002; Boss & Durisen 2005), clumps of infalling material impacting the solar nebula (Boss & Graham 1993), and planetesimals moving at supersonic speeds through the solar nebula (Weidenschilling et al. 1998).

From the perspective of the jet-flow model, a relict CAI can be incorporated into a chondrule if the CAI is ejected to the outer parts of the nebula and subsequently moves back to the outflow region, adjacent to the Sun, where chondrules are now the main products of the jet flow. There are at least two mechanisms that can move the CAI back to the jet flow region: (1) the average accretion flow of the nebula onto the Sun and (2) the infall of the CAI due to aerodynamic drag (Weidenschilling 1977). Disks around classical T Tauri stars (CTTSs) have an observed accretion lifetime of 1–10 Myr (Calvet et al. 2000; D'Alessio et al. 2005). This implies an approximate, average disk lifetime of around 5 Myr. In turn, an average solid particle in an average CTTS disk will have an approximate lifetime against accretion into the Sun of around 2.5 Myr. Using aerodynamic drag calculations given in Weidenschilling (1977), but the original Epstein's gas-drag coefficient[12] (Epstein 1924), we find that aerodynamic drag causes 20 and 100 μm diameter CAIs to move toward the Sun on timescales of 10 and 1 Myr, respectively, where these timescales are averaged over the entire solar nebula. The accretion infall timescales would be the approximate upper limits for the average residence time of a solid particle in the nebula. Thus, within the context of the jet-flow model, the upper limit on the average time difference between the observed relict CAIs and host chondrules is approximately 1–2.5 Myr, which is consistent with the observed age difference between relict CAIs and their host chondrules.

According to the shock model, the CAIs would have to be present as freely floating objects at about 2–3 AU from the Sun about 2 Myr after their formation. This could have been achieved in the turbulent solar nebula (Cuzzi et al. 2003, 2005). Assuming that CAIs formed in a hot inner (turbulent) nebula and using analytical models of nebula evolution and particle diffusion, Cuzzi et al. (2003, 2005) showed that the outward radial diffusion in a weakly turbulent nebula can overcome inward drift and prevent significant numbers of CAI-sized particles from being lost into the Sun for times on the order of 10^6 yr. Alternatively, the CAIs could have agglomerated into large, kilometer-sized bodies, which prevented them from falling into the Sun. After 2 Myr some of the CAIs would have to be released from the planetesimals either by collisions between planetesimals or by an ablative process (Genge 2000).

Although the results presented here cannot invalidate any particular model, it would appear that the shock model requiring an extra stage of agglomeration and disintegration of planetesimals is more complicated.

[12] The gas-drag equation of Liffman & Brown (1996) is $C_{dg} = [16/(3\sqrt{\pi})](1/s)C$, where C_{dg} is the gas-drag coefficient, s is the thermal Mach number, and the constant $C = 1 + \pi/8 \approx 1.393$ for spheres that are perfect thermal conductors and $C = 1 + 9\pi/64 \approx 1.442$ for spheres that are perfect insulators. In Weidenschilling (1977), C is set equal to 1, which is physically incorrect; $C = 1.393$ is the more physically correct value (for details see Liffman & Toscano 2000).

5. SUMMARY AND CONCLUSIONS

We have identified five examples of CAIs that were incorporated into chondrules when the chondrules formed and that still retain some of their primary characteristics. Mineralogy and O isotopes suggest that four of these CAIs were "normal" CAIs like those found in many types of primitive chondrites. Aluminum-magnesium systematics in Adelaide CAI 9d show that the chondrule melting event took place $\geq$2 Myr after the CAI formed. This is the first time that such an interpretation does not depend on an assumption of the homogeneous distribution of ^{26}Al in the chondrule-forming region. Isotopic data for the three other "normal" CAIs can be interpreted in a similar way, although their interpretations are not unique. The fifth CAI (Acfer CAI 17) appears to have formed with a ^{26}Mg deficit and no ^{26}Al, and thus it is an unusual CAI. The lack of ^{26}Al means that we cannot put a constraint on the time difference between CAI and chondrule formation for this object.

The thin section of PAT 91546 used in this study was provided by NASA Johnson Space Center. This work was supported by NASA grants NAG5-10610 (A. N. Krot, PI), NAG5-4704 (K. D. McKeegan, PI), NAG5-11543 (G. R. Huss, PI), NAG5-10523 (I. D. Hutcheon, PI), and NAG5-11591 (K. Keil, PI), and was performed under the auspices of the Department of Energy by LLNL under contract W-7405-ENG-48. The UCLA ion microprobe laboratory is partially supported by a grant from the NSF Instrumentation and Facilities program. This is Hawai'i Institute of Geophysics and Planetology publication 1422 and School of Ocean and Earth Science and Technology publication 6706.

REFERENCES

Aléon, J., Krot, A. N., & McKeegan, K. D. 2002, Meteoritics Planet. Sci., 37, 1729
Amelin, Y., Krot, A. N., Hutcheon, I. D., & Ulyanov, A. A. 2002, Science, 297, 1678
Amelin, Y., Krot, A. N., Russell, S. S., & Twelker, E. 2004, Geochim. Cosmochim. Acta, 68, A759
Bischoff, A., & Keil, K. 1984, Geochim. Cosmochim. Acta, 48, 693
Bizzarro, M., Baker, J., & Haack, H. 2004, Nature, 431, 275
Boss, A. P., & Durisen, R. H. 2005, in ASP Conf. Ser. 341, Chondrites and the Protoplanetary Disk, ed. A. Krot, E. Scott, & B. Reipurth (San Francisco: ASP), 821
Boss, A. P., & Graham, J. A. 1993, Icarus, 106, 168
Brearley, A. J. 1990, Geochim. Cosmochim. Acta, 54, 831
Calvet, N., Hartmann, L., & Strom, S. 2000, in Protostars and Planets IV, ed. V. Mannings, A. Boss, & S. Russell (Tucson: Univ. Arizona Press), 377
Catanzaro, E., Murphy, T., Garner, E., & Shields, W. 1966, J. Res. NBS A, 70, 453
Clayton, R. N. 2002, Nature, 415, 860
Clayton, R. N., et al. 1984, Geochim. Cosmochim. Acta, 48, 535
Cuzzi, J. N., Ciesla, F. J., Petaev, M. I., Krot, A. N., Scott, E. R. D., & Weidenschilling, S. J. 2005, in ASP Conf. Ser. 341, Chondrites and the Protoplanetary Disk, ed. A. Krot, E. Scott, & B. Reipurth (San Francisco: ASP), 732
Cuzzi, J. N., Davis, A., & Dobrovolskis, A. 2003, Icarus, 166, 385
Cuzzi, J. N., & Zahnle, K. J. 2004, ApJ, 614, 490
D'Alessio, P., Calvet, N., & Woolum, D. S. 2005, in ASP Conf. Ser. 341, Chondrites and the Protoplanetary Disk, ed. A. Krot, E. Scott, & B. Reipurth (San Francisco: ASP), 353
Desch, S. J., & Connolly, H. C. 2002, Meteoritics Planet. Sci., 37, 183
Epstein, P. 1924, Phys. Rev., 23, 710
Fahey, A., Zinner, E., Crozaz, G., & Kornacki, A. 1987, Geochim. Cosmochim. Acta, 51, 3215
Genge, M. 2000, Meteoritics Planet. Sci., 35, 1143
Goswami, J. N., Marhas, K. K., Chaussidon, M., Gounelle, M., & Meyer, B. S. 2005, in ASP Conf. Ser. 341, Chondrites and the Protoplanetary Disk, ed. A. Krot, E. Scott, & B. Reipurth (San Francisco: ASP), 485
Gounelle, M., Shu, F., Shang, H., Glassgold, A., Rehm, K., & Lee, T. 2001, ApJ, 548, 1051
Greshake, A. 1997, Geochim. Cosmochim. Acta, 61, 437
Hashizume, K., & Chaussidon, M. 2005, Nature, 434, 619
Huneke, J., Armstrong, J., & Wasserburg, G. J. 1983, Geochim. Cosmochim. Acta, 47, 1635
Huss, G. R., Hutcheon, I. D., Krot, A. N., & Tachibana, S. 2002, Lunar Planet. Sci. Conf., 34, 1802
Huss, G. R., MacPherson, G. J., Wasserburg, G. J., Russell, S. S., & Srinivasan, G. 2001, Meteoritics Planet. Sci., 36, 975
Iida, A., Nakamoto, T., Susa, H., & Nakagawa, Y. 2001, Icarus, 153, 430
Ireland, T., Fahey, A., & Zinner, E. 1991, Geochim. Cosmochim. Acta, 55, 367
Itoh, S., & Yurimoto, H. 2003, Nature, 423, 728
Jones, R. H., Lee, T., Connolly, H. C., Jr., Love, S., & Shang, H. 2000, in Protostars and Planets IV, ed. V. Mannings, A. Boss, & S. Russell (Tucson: Univ. Arizona Press), 927
Kimura, M., El Goresy, A., Palme, H., & Zinner, E. 1993, Geochim. Cosmochim. Acta, 57, 2329
Kita, N. T., Huss, G. R., Tachibana, S., Amelin, Y., Nyquist, L. E., & Hutcheon, I. D. 2005, in ASP Conf. Ser. 341, Chondrites and the Protoplanetary Disk, ed. A. Krot, E. Scott, & B. Reipurth (San Francisco: ASP), 558

Kita, N. T., Nagahara, H., Togashi, S., & Morishita, Y. 2000, Geochim. Cosmochim. Acta, 64, 3913
Krot, A. N., Fagan, T. J., Keil, K., McKeegan, K. D., Sahijpal, S., Hutcheon, I. D., Petaev, M. I., & Yurimoto, H. 2004a, Geochim. Cosmochim. Acta, 68, 2167
Krot, A. N., Hutcheon, I. D., & Huss, G. R. 2001, Meteoritics Planet. Sci., 36, A105
Krot, A. N., Hutcheon, I. D., & Keil, K. 2002a, Meteoritics Planet. Sci., 37, 155
Krot, A. N., & Keil, K. 2002, Meteoritics Planet. Sci., 37, 91
Krot, A. N., Libourel, G., & Chaussidon, M. 2004b, Lunar Planet. Sci. Conf., 35, 1389
Krot, A. N., MacPherson, G. J., Ulyanov, A. A., & Petaev, M. I. 2004c, Meteoritics Planet. Sci., 39, 1517
Krot, A. N., McKeegan, K. D., Leshin, L. A., MacPherson, G. J., & Scott, E. R. D. 2002b, Science, 295, 1051
Krot, A. N., Sahijpal, S., McKeegan, K. D., Weber, D., Ulyanov, A. A., Petaev, M. I., Meibom, A., & Keil, K. 1999, Meteoritics Planet. Sci., 34, A69
Krot, A. N., & Wasson, J. T. 1994, Meteoritics, 29, 707
Krot, A. N., Yurimoto, H., Hutcheon, I. D., & MacPherson, G. J. 2005a, Nature, 434, 998
Krot, A. N., et al. 2005b, ApJ, 622, 1333
LaTourrette, T., & Hutcheon, I. D. 1999, Lunar Planet. Sci. Conf., 30, 2003
LaTourrette, T., & Wasserburg, G. J. 1997, Lunar Planet. Sci. Conf., 28, 781
Lee, T., & Papanastassiou, D. 1974, Geophys. Res. Lett., 1, 225
Leshin, L. A., McKeegan, K. D., Engrand, C., Zanda, B., Bourot-Denise, M., & Hewins, R. H. 1998, Meteoritics Planet. Sci., 33, A93
Liffman, K. 1992, Icarus, 100, 608
Liffman, K., & Brown, M. 1996, in Chondrules and the Protoplanetary Disk, ed. R. Hewins, R. Jones, & E. Scott (Cambridge: Cambridge Univ. Press), 285
Liffman, K., & Toscano, M. 2000, Icarus, 143, 106
Lin, Y., & Kimura, M. 1998, Meteoritics Planet. Sci., 33, 435
Lyons, J. R., & Young, E. D. 2005, Nature, 435, 317
MacPherson, G. J., Davis, A. M., & Grossman, J. N. 1989, Meteoritics, 24, 297
MacPherson, G. J., Davis, A. M., & Zinner, E. K. 1995, Meteoritics, 30, 365
MacPherson, G. J., Wark, D. A., & Armstrong, A. 1988, in Meteorites and the Early Solar System, ed. J. Kerridge & M. Matthews (Tucson: Univ. Arizona Press), 746
Marhas, K. K., Hutcheon, I. D., Krot, A. N., & Goswami, J. N. 2000, Meteoritics Planet. Sci., 35, A102
McKeegan, K. D., Greenwood, J., Leshin, L. A., & Cozarinsky, M. 2000, Lunar Planet. Sci. Conf., 31, 2009
McKeegan, K. D., Leshin, L. A., Russell, S. S., & MacPherson, G. J. 1998, Science, 280, 414
Meibom, A., Desch, S. J., Krot, A. N., Cuzzi, J. N., Petaev, M. I., Wilson, L., & Keil, K. 2000, Science, 288, 839
Misawa, K., & Fujita, T. 1994, Nature, 368, 723
Misawa, K., & Nakamura, N. 1988, Nature, 334, 47
Mostefaoui, S., Kita, N. T., Togashi, S., Tachibana, S., Nagahara, H., & Morishita, Y. 2002, Meteoritics Planet. Sci., 37, 421
Pouchou, J. L., & Pichoir, F. 1985, in Microbeam Analysis, ed. J. T. Armstrong (San Francisco: San Francisco Press), 104
Russell, S. S., Huss, G. R., Fahey, A., Greenwood, R., Hutchison, R., & Wasserburg, G. J. 1998, Geochim. Cosmochim. Acta, 62, 689
Russell, S. S., Srinivasan, G., Huss, G. R., Wasserburg, G. J., & MacPherson, G. J. 1996, Science, 273, 757
Shu, F., Shang, H., Gounelle, M., Glassgold, A., & Lee, T. 2001, ApJ, 548, 1029
Shu, F., Shang, H., & Lee, T. 1996, Science, 271, 1545
Simon, S. B., Davis, A. M., & Grossman, L. 1997, Meteoritics Planet. Sci., 32, A121
Wark, D. A., & Lovering, J. F. 1977, Proc. Lunar Sci. Conf., 8, 95
Weber, D., Zinner, E., & Bischoff, A. 1995, Geochim. Cosmochim. Acta, 59, 803
Weidenschilling, S. J. 1977, MNRAS, 180, 57
Weidenschilling, S. J., Marzari, F., & Hood, L. L. 1998, Science, 279, 681
Wood, J. A. 1996, Lunar Planet. Sci. Conf., 27, 1453
Young, E. D., Simon, J. I., Galy, A., Russell, S. S., Tonui, E., & Lovera, O. 2005, Science, 308, 223
Yurimoto, H., & Kuramoto, K. 2004, Science, 305, 1763